

Valorization of mixed plastics waste for the synthesis of flexible superhydrophobic films

Junaid Saleem, Zubair Khalid Baig Moghal, Luyi Sun, Gordon McKay

Item type

Journal Contribution

Terms of use

This work is licensed under a [CC BY 4.0](#) license

This version is available at

https://manara.qnl.qa/articles/journal_contribution/Valorization_of_mixed_plastics_waste_for_the_synthesis_of_flexible_superhyd

Access the item on Manara for more information about usage details and recommended citation.

Posted on Manara – Qatar Research Repository on

2024-01-09



Valorization of mixed plastics waste for the synthesis of flexible superhydrophobic films

Junaid Saleem¹ · Zubair Khalid Baig Moghal² · Luyi Sun^{3,4,5} · Gordon McKay¹

Received: 2 August 2023 / Revised: 28 December 2023 / Accepted: 1 January 2024 / Published online: 9 January 2024
© The Author(s) 2024

Abstract

Superhydrophobic surfaces are typically created by enhancing nanoscale roughness or incorporating anti-wetting additives like silanes, nanoparticles, or fluorinated compounds. Limited by the availability of nano-structured templates, simple fabrication, flexibility of the material, and cost-effectiveness, the quest to synthesize superhydrophobic films remains challenging. Herein, we report the valorizing of mixed plastic waste for the synthesis of flexible superhydrophobic films via open-loop recycling. We focused on improving the nanoscale surface roughness of the material by using a series of steps including selective dissolution, thermally induced phase separation, controlled spin-casting, and annealing. We synthesized a two-layered superhydrophobic film with high surface roughness and sufficient mechanical strength, making it suitable for use as a free-standing material. The contact and sliding angles were found to be 159° and 4°, respectively, with an RMS (root mean square) surface roughness of 228 nm. This approach is demonstrated with mixtures of high-density polyethylene (HDPE), low-density polyethylene (LDPE), and polypropylene (PP), which are among the most abundant components of post-consumer plastic waste. Life cycle assessments show that synthesized superhydrophobic films have lower carbon dioxide emissions and embodied energy than virgin PE and PP derived from petroleum. Our design strategy not only yields a superhydrophobic product but also provides an alternative to plastic waste recycling by bypassing cost-intensive sorting techniques.

Keywords Superhydrophobic films · Waste plastic · Valorization · Contact angle · Life-cycle assessment

1 Introduction

Plastic waste accounts for approximately 13% of the total municipal solid waste, with a significant proportion ending up in the ocean, where seabirds and fish are likely to ingest

approximately 13 million tons of plastic annually [1, 2]. According to conservative estimates, if current trends continue, the oceans will contain more plastic than fish by weight by 2050 [3]. Despite intensive recycling campaigns around the globe, less than 10% of around 400 million tons of plastic produced annually makes it to the recycled stream while only 10% of the 20,000 plastic bottles produced every second will eventually be recycled [4–6]. Thus, making it imperative that we find a solution to the waste-plastic recycling conundrum [7–9].

Mechanical recycling is presently the most widely employed method for repurposing plastic waste [10, 11]. However, the mechanical recycling faces constraints when dealing with plastic waste streams that encompass diverse plastic types. Additionally, plastics with surface coatings and modifications are difficult to upcycle, and the market for downcycled products is volatile, further reducing the effectiveness of mechanical recycling [12]. Chemical recycling, on the other hand, offers a more lucrative alternative, as it is better suited to handling a mixed stream of plastic waste. However, chemical recycling is more complex and requires high capital investment and large volumes of plastic waste

Junaid Saleem and Zubair Khalid Baig Moghal have equal contribution.

✉ Junaid Saleem
jsaleem@hbku.edu.qa

¹ Division of Sustainable Development, College of Science and Engineering, Hamad Bin Khalifa University, Qatar Foundation, Doha, Qatar

² Center for Advanced Materials, Qatar University, Doha, Qatar

³ Department of Chemical and Biomolecular Engineering, University of Connecticut, Storrs, CT 06269, USA

⁴ Department of Biomedical Engineering, University of Connecticut, Storrs, CT 06269, USA

⁵ Polymer Program, Institute of Materials Science, University of Connecticut, Storrs, CT 06269, USA

to be cost-effective [6, 13, 14]. Therefore, finding a sustainable recycling method that can handle mixed plastic waste streams with a competitive advantage over mechanical recycling is a pressing priority.

To combat this issue, upcycling strategies have been developed, which involve the use of plastic waste as a feedstock for synthesizing value-added products, being molecules, materials, or polymers [15–17]. While these technologies have been effective in reducing plastic pollution to some extent [18–20], they tend to use isolated plastic waste or single plastic streams. Since post-consumer plastic waste is mixed, it becomes difficult to separate and identify individual polymers [21–23]. This complexity makes separation methods expensive and time-consuming, limiting the recycling or upcycling of these materials [24–26]. Hence, upcycling process that converts mixed plastics into a valuable product without sorting could bypass this limitation [27]. Our research group has identified one such solution in which mixed plastics waste is converted into free-standing superhydrophobic films.

The concept of superhydrophobic coating entails a surface that exhibits a water contact angle exceeding 150° and a sliding angle lower than 5° [28–31]. Apart from their application in water protection, flexible superhydrophobic films also serve as matrices for electromagnetic composites [32–35]. In order to achieve such surfaces, several commonly employed materials include fluoro-polysiloxane and polydimethylsiloxane [36], black iron oxide nanoparticles (NPs) [37], titanium dioxide, and stoichiometric salinization [38, 39], composite microspheres consisting of polystyrene and silicon dioxide [40], silicon dioxide combined with epoxy resin [41], fluorinated nanodiamonds [42], silicon dioxide nanoparticles embedded within electro-spun fibrous mats [43], as well as cellulose-based derivatives [44].

While these materials yield superhydrophobic surfaces, they contain fluorinated and/or silane compounds which increase the overall cost of the material. Utilizing plastic waste, on the other hand, provides a cheaper alternative but producing a free-standing superhydrophobic surface remains a challenge. There are two approaches in creating hydrophobicity: (a) grafting of a chemical that possesses anti-wetting properties, and (b) creating surface roughness by altering the morphology [45].

In this work, we present a strategy whereby mixed plastics were converted into free-standing superhydrophobic films with high surface roughness through selective dissolution, thermally induced phase separation, and annealing. The initial dissolution step prepared a dilute polymer solution of polyolefins which overcame the compatibility issue among them by allowing the polymeric chains to exfoliate and intertwine as they became fluid in the dissolved state. The solution was then spin-cast maintaining controlled thickness on a glass substrate and was cooled by keeping the plate in air to induce the phase separation. The resultant layer had a highly rough surface that facilitated hydrophobicity. However, its

mechanical strength was found to be inadequate and could not be used as a free-standing material, rendering it unsuitable for practical applications. To overcome this limitation, the layer was subjected to controlled heating and cooling to crystallize and strengthen the polymeric structure while closing the pores. Unfortunately, this process led to a significant reduction in surface roughness, resulting in a lower contact angle. To address this issue, a second layer was applied on top of the base-layer using the same spin-casting method, but with modifications to preserve its porous structure, surface roughness, and superhydrophobicity. The bottom layer served as a substrate for the top layer, aiding in its proper formation. Additionally, it provided support and strength, contributing to the overall structural integrity of the film. This approach was demonstrated with mixtures of high-density polyethylene (HDPE), low-density polyethylene (LDPE), and polypropylene (PP), which are among the most abundant components of postconsumer plastic waste. Lastly, a life cycle assessment (LCA) was conducted to compare the environmental impacts of superhydrophobic film produced from plastic waste with virgin pellets of PP and PE produced from petroleum source.

The present solution expands its applicability by enabling the precise development of superhydrophobic films through the alteration of layers' thicknesses based on specific application requirements. In instances where high mechanical strength is a critical requirement, the base layer thickness can be increased from 30 to 175 μm . Similarly, the thickness of the top layer can be increased from 10 to 100 μm . Figure 1 illustrates the overview of the superhydrophobic surface using polyolefin.

2 Experimental section

2.1 Material and reagents

p-Xylene was procured from Sigma Aldrich and used without additional refining. High-density polyethylene (HDPE), low-density polyethylene (LDPE), and polypropylene (PP) waste containers were collected locally. A 5 cm \times 5 cm plain glass plate was cut to size and used as the substrate, mounted on the spin coater's chuck, which was customized by Ossila. Spin-casting was carried out using a spin coater from Ossila. A hot air oven made of MINO/30/TDIG by Genlab Ltd was used for heating and annealing. Hot plate annealing was carried on Heidolph magnetic hotplate stirrer. Friction/peel tester Lloyd Instruments Ltd Bognor Regis, UK, was used for tensile strength and modulus calculations. Scanning electron microscopy (SEM) images were captured with FEI Quanta650FEG. Differential scanning calorimetry (DSC) was used to determine the thermal behavior of HDPE-based hydrophobic thin films

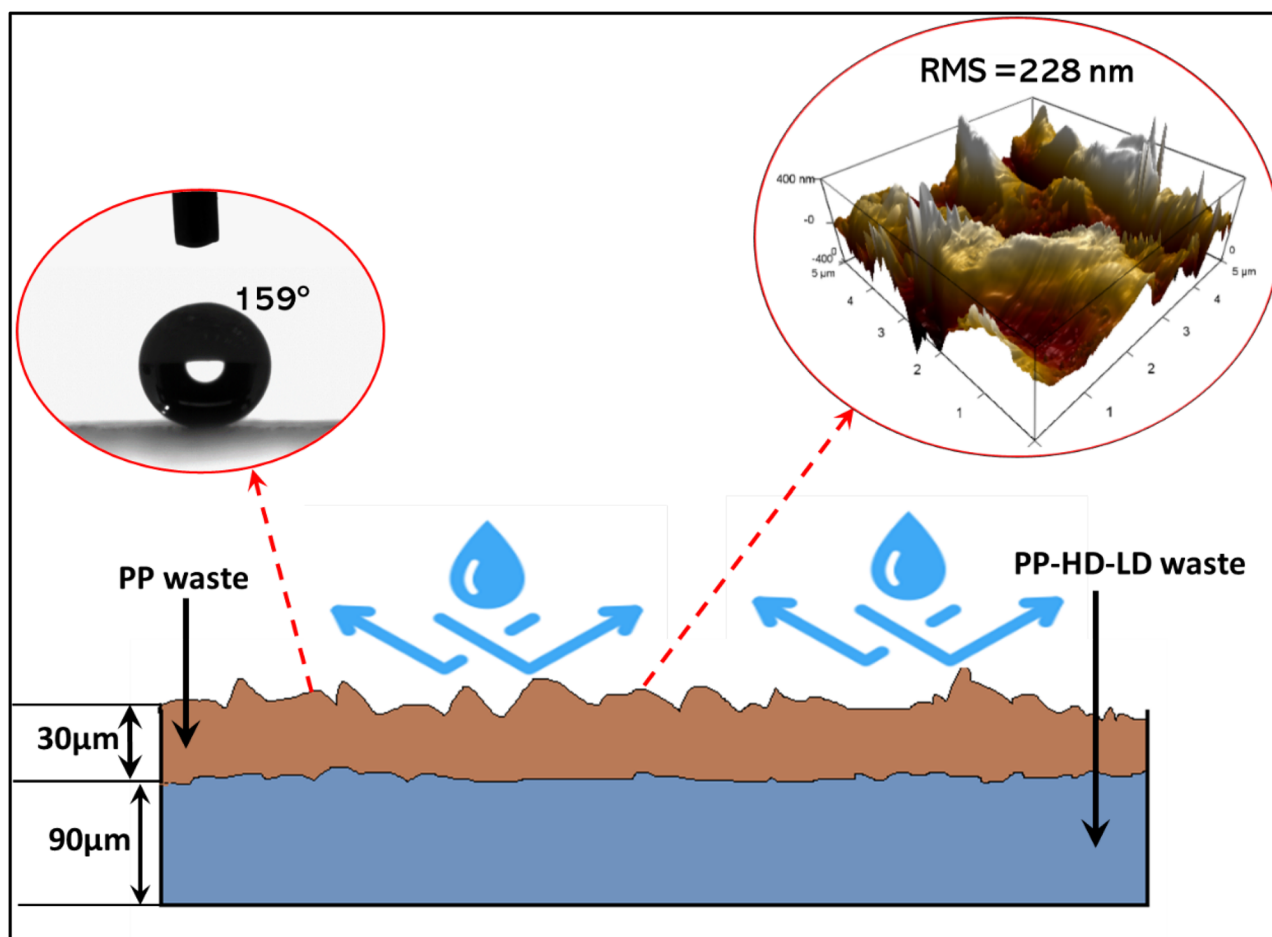


Fig. 1 Overview of the superhydrophobic surface using polyolefin

and to evaluate the changes in enthalpy before and after heating. Thin films were heated in a crucible at 10 °C/min under nitrogen in the 25–800 °C temperature range using Q50 Perkin Elmer thermal analyzer. X-ray diffraction (XRD) measurements were measured using PANalytical Empyrean multipurpose XRD by Malvern Panalytical, Malvern, UK. X-ray photoelectron spectroscopy (XPS) was measured using the Thermo Fischer Escalab 250XI platform. A monochromated X-ray source (Al K α : 1486.6 eV) is used. Surface morphology analysis was conducted through Atomic force microscopy (AFM) Park NX10 in order to understand the surface roughness of thin films. Fourier-transform infrared spectroscopy (FTIR) was carried out using the PerkinElmer Frontier instrument. Profilometry imaging was carried out using a Leica DCM8 microscope. The optical contact angle was calculated using OCA 35, Dataphysics instruments GmbH – Filderstadt, Germany. Porosity was calculated using the wet porosity method, where the difference between the weight of the thin film with ethanol and the weight of the thin film was converted into the volume by dividing it by

density. Thickness was measured with a micrometre and cross-referred with Deflesko FS3 PosiTector 6000 using an iron metal base.

2.2 Methods

2.2.1 Preparation of HDPE-blend

Two solutions, solution 1 and solution 2 were prepared simultaneously. Solution 1 was prepared using 10 g of plastic waste including LDPE, HDPE, and PP in equal quantities and dissolving them in 100 ml of p-xylene under reflux conditions of 130 °C for a time of 20 min. Solution 2 was prepared using 10 g of HDPE waste and dissolving it in 100 ml of p-xylene under reflux conditions of 130 °C for 20 min. A 25 cm² shaped glass plate (substrate) was cleaned and then heated to a temperature of 120 °C before being placed on a spin coater chuck. The hot polymer solution-1 was poured in a specific amount on the substrate and spin-coated at a gradient speed of 400 rpm for 10 s, followed by 1000 rpm for 60 s, followed by 3000 rpm for 60 s. The excess solvent

and polymer solution were collected from the drain for recycling. After completion of the spin casting, the substrate was separated from the chuck and the base layer was heated to a temperature of 170 °C for a period of 30 s on a Heidolph hot plate. Afterward, the hot glass plate with a polymer base layer was cooled to 120 °C and placed on the chuck, and the hot polymer solution-2 in a specific amount was poured over the hot base layer and spun at similar speeds. After the spin casting, the glass substrate with combined top and base layers was detached from the chuck and the film was peeled off easily from the substrate resulting in a superhydrophobic thin film.

2.2.2 Preparation of PP-blend

Two solutions, solution 1 and solution 2 were prepared simultaneously. Solution 1 was prepared using 10 g of plastic waste including LDPE, HDPE, and PP in equal quantities and dissolving them in 100 ml of p-xylene under reflux conditions of 130 °C for a time of 20 min. Solution 2 was prepared using 10g of polypropylene waste and dissolving it in 100 ml of p-xylene under reflux conditions of 130 °C for 20 min. A 25 cm² shaped glass plate (substrate) was cleaned and then heated to a temperature of 120 °C before being placed on a spin coater chuck. The hot polymer solution-1 was poured in a specific amount on the substrate and spin-coated at a gradient speed of 400 rpm for 10 s, followed by 1000 rpm for 60 s, followed by 3000 rpm for 60 s. The excess solvent and polymer solution were collected from the drain for recycling. After completion of the spin casting, the substrate was separated from the chuck and the base layer was heated to a temperature of 170 °C for a period of 30 s on a Heidolph hot plate. Afterward, the hot glass plate with a polymer base layer was cooled to 120 °C and placed on the chuck, and the hot polymer solution-2 in a specific amount was poured over the hot base layer and spun at similar speeds. After the spin casting, the glass substrate with combined top and base layers was detached from the chuck and the film was peeled off easily from the substrate resulting in a superhydrophobic thin film. Table 1 and Fig. S1

shed light on details of the fabrication strategy and techniques used in this study.

2.2.3 Fabrication strategy of free-standing superhydrophobic thin films

Adhesion between two layers holds significant importance in the context of thin film development. Initially, during our endeavor to create a hydrophobic thin film, we applied a first layer on the substrate and tried to separate it from the substrate. But because of weak strength and loosely connected polymer chains, it cannot be peeled off in one piece, instead, chipping occurred. Thus it could not be used as an independent sheet. However, the surface was rough enough to exhibit superhydrophobicity.

As part of our second fabrication strategy, we decided to heat the base layer after its application. Then we subjected the substrate and the first layer to heating. Upon heating the polymer chains becomes soft and interconnected with the adjacent polymer chains by the enhancement of dispersion forces. This heating process aimed to close all the pores and reinforce the first polymer layer, thereby facilitating easy removal from the spin coat plate. We could easily separate the first layer from the substrate but it is not superhydrophobic in property. We termed this first layer as base layer. Implementing this second fabrication strategy, involving the heating of the base layer, yielded a free-standing thin film.

Thus, we introduced multilayer application so that the top layer acts as a superhydrophobic coating and the base layer provides support. In the multilayer sheets, initially, we poured solution 2 on base layer when the base layer was at room temperature or cold. We observed chipping of the top layer, as there was poor adhesion between the top layer and the base layer. This poor adhesion is because the polymer in the base layer was in rigid and solid form, and the newly added layer is in molten form, and change in phases caused the interconnection between the newly added layer and the rigid layer to be weak. Thus there was chipping and poor adhesion. However, the issue of adhesion remained unresolved.

Table 1 Multilayered hydrophobic thin films fabrication strategy

Formulation name	Fabrication strategy	Base layer (Solution 1)		Top Layer (Solution 2)	Techniques used
HD-Blend	HDPE layering on waste polymer blend	Polymer blend		High-density polyethylene (HDPE)	Spin casting and annealing
		HDPE	33.33 %		
		LDPE	33.33 %		
		PP	33.33 %		
PP-Blend	PP layering on waste polymer blend	Polymer blend		Polypropylene (PP)	Spin casting and annealing
		HDPE	33.33 %		
		LDPE	33.33 %		
		PP	33.33 %		

In order to address the adhesion problem, we developed a third fabrication strategy. This approach involved heating the base layer to enhance the strength of the thin film and applying the top layer when the base layer reached a temperature of 120 °C. Then we kept the base layer at a high temperature of 120 °C, but below the boiling point of the solvent. Consequently, the resulting thin film exhibited improved adhesion between its two layers, and upon removal from the spin coat, it could be easily peeled off. This good adhesion is because when the base layer is hot and solution 2 is poured, both the polymer will be in a molten and soft state, thus the adhesion between the base layer and the newly applied layer is excellently achieved.

After which, the combined base layer and top layer were detached from the substrate resulting in a superhydrophobic thin film. Therefore, the third fabrication strategy proved successful in the development of free-standing, well-fused bilayer superhydrophobic thin films.

3 Results and discussion

3.1 Morphological analysis of hydrophobic thin films

Figure 2 illustrates the results of an SEM examination conducted to investigate the internal structure of HD-Blend

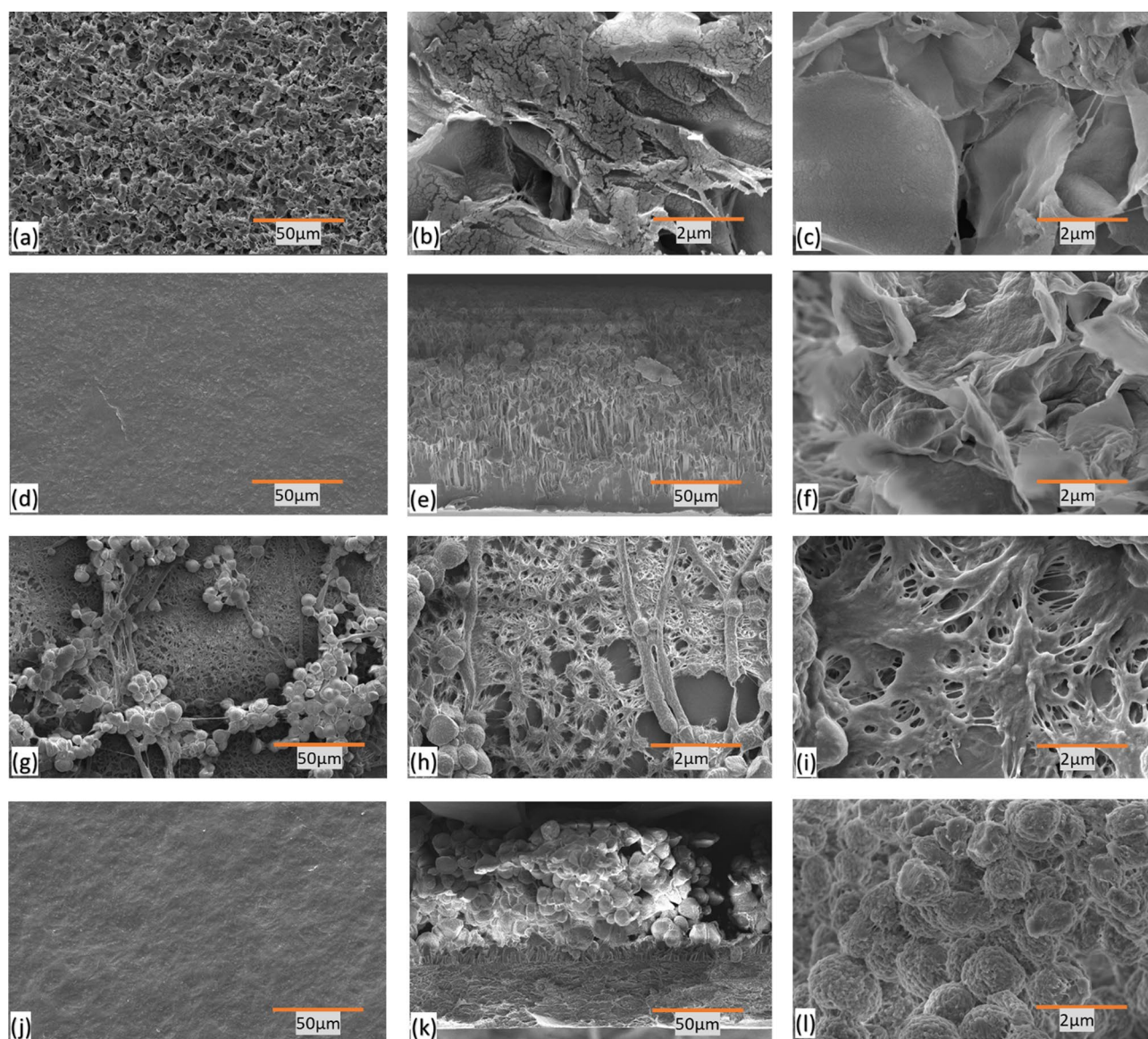


Fig. 2 SEM images of **a** HD-blend top surface **b** HD-blend top surface (zoomed version) **c** HD-Blend top surface zoomed after 5 min of heating 120 °C **d** HD-blend bottom surface after complete heating **e** HD-blend cross-section overview **f** HD-blend cross-section zoomed

version; **g** PP-blend top surface **h** PP-blend top surface (zoomed version) **i** PP-Blend top surface zoomed after 5 min of heating 120 °C **j** PP-blend bottom surface after complete heating **k** PP-blend cross-section overview; **l** PP-blend cross-section zoomed version

thin films. In Fig. 2a, the top surface of HD-Blend exhibits a petal-like structure that extends from the bottom and spreads outwards from the top, resembling a flower. Figure 2b is the zoomed-in versions of the top surface, highlighting the surface roughness and the presence of spikes. The formation of spikes on the surface contributes to the water repellency as it helps in the suspension of water droplets due to the formation of airpockets, resulting in a contact angle of 148° for HD-Blend.

Figure 2c showcases the top surface of HD-Blend after being heated for five min at 120°C . As a result of the heating, the polymer starts to melt, leading to a reduction in the spikes and a smoother surface. The smoother surface of the thin film, when tested for water repellency, yields a contact angle of 138° . This indicates that heating causes the spikes to diminish, resulting in decreased water repellency. Figure 2d displays a micrograph of the fully heated surface (base layer) of HD-Blend. It is evident that complete heating eliminates all spikes and completely reduces surface roughness, resulting in minimal water repellency with a contact angle of 108° .

In addition, Fig. 2e–f presents cross-sectional views of HD-Blend, displaying the overview and zoomed versions, respectively. These micrographs reveal the formation of a wavy pattern between the layers of HD-Blend, which contributes to its water repellency.

Figure 2g–l depicts the findings of an SEM examination conducted to investigate the internal structure of thin films made of PP-blend. In Fig. 2g, the top surface of the PP-Blend film exhibits two types of structures: weblike structures and spherical structures. The weblike structures help connect the top layer and the base layer during the annealing process. On the other hand, the spherical structures helped in providing superhydrophobicity.

With a closer view of the top surface of the PP-Blend film in Fig. 2h, it becomes apparent that the formation of spikes has occurred on both the weblike and spherical structures, leading to an improvement in water repellency. The main reason behind the highly improved water-repellent properties in the PP-Blend film is the formation of these spike extrusions. These are formed due to the thermally-induced phase separation of polymer and solvent. This is evident from the contact angle of 159° in the case of PP-Blend (see contact angle section). However, when the film is heated for 5 min at 120°C , these spikes diminish, resulting in a reduction in water repellency, as shown in Fig. 2i. Similarly, Fig. 2j displays micrographs of the PP-Blend film after complete heating, revealing that heating softens the polymer, diminishing all the spikes and significantly reduced the surface roughness, thereby considerably reducing the water-repellent properties.

Figure 2k provides a cross-sectional overview of the PP-Blend film. It is evident that the bubbly (spherical) structure

of pure PP (top layer) is visibly fusing together the top layer with the base layer through the weblike structure. For a closer look at the cross-sectional overview of the PP-Blend film, Fig. 2l offers a zoomed-in version. This image demonstrates the presence of spherical, bubbly structures with spikes all over them, which are responsible for the superhydrophobic properties of the PP-Blend film. Such spherical structures resembling bubbles can also be found on the surface of sacred lotus leaves [46]. These leaves have micro-level roughness, which is due to the presence of spikes on their spherical structures, resulting in water contact angles of up to 170° . The air trapped between the droplets and the wax crystals on the plant surface minimizes the contact area, contributing to the high contact angle [45].

3.1.1 Observation regarding the surface morphological analysis

Further, it was necessitated to learn the parameters that affect the roughness and surface morphology. The superhydrophobicity of a polymeric film was influenced by changes in viscosity and speed of the spin-casting rotation. Initially, a more viscous polymer solution resulted in thick films because of more deposition of polymer content and a less viscous polymer solution resulted in thin films because of deposition of less polymer content. In addition, high speed reduces the thickness, and low speed increases the thickness. To simplify the alterations, we have considered spinning at four different conditions, (a) more viscous solution at low speed, (b) high viscosity at low speed, (c) low viscosity at high speed, and (d) low viscosity at low speed.

With the modification in viscosity and speed, amendments in various parameters were observed that played significant phenomena in achieving excellent superhydrophobicity and water contact angles. The observed parameters were pore size, pore size distribution, homogeneity, roughness, stretching, spiky protrusions, etc. We will study each parameter affected by these conditions.

- (a) Pore size and Pore size distribution: Pore size and Pore size distribution: Firstly, when a highly viscous polymer solution was spun at low speed, more polymer particles remain on the substrate. With a low proportion of solvent molecules in a highly viscous solution and the elimination of the solvent molecules upon drying, we achieved a very low phase-separated area. These low phase-separated regions result in very small micropores with very small pore sizes ranging from $0.1\text{--}0.5\mu\text{m}$ and small pore size distribution. A high viscous solution at a low speed allows more polymer particles to remain on the substrate compared to a low viscous solution at a low speed, which is attributed to more polymer proportion. Secondly, when a highly viscous polymer solution

was spun at high speed, more polymer particles are expelled from the substrate because of enhancement in the centrifugal forces and increased polymer mass ratio. With more expulsion of the polymer molecules, the polymer molecules are stretched and space between the polymer molecules is enhanced resulting in an intense increase in phase-separated area. These increased phase-separated regions resulted in a very high pore size ranging between 20 μm and 500 μm , and high pore size distribution. However, a low viscous solution at a low speed allows more polymer particles to remain on the substrate compared to a low viscous solution at a higher speed. This low viscous solution at low speed resulted in a small pore size ranging from 0.5–5 μm with a relatively larger pore size distribution compared to a more viscous solution at low speed. Further, a low viscous solution at high speed resulted in large pore sizes ranging from 5 μm –200 μm and lead to a relatively smaller pore size distribution compared to a more viscous solution at a high speed. The pore sizes and pore distribution play a significant role in maintaining the contact angle. The air inside the air pockets of the pores creates tension, suspends the water droplet over the surface and resists the contact of water droplets with the base layer. The tension created by the air pockets should dominate the gravitational tension of the water to achieve a superhydrophobic surface. A large pore size with large pore size distribution (achieved through more viscous at high speed) and a large pore size with a small pore size distribution (achieved through less viscous at high speed) result in a decrease in contact angle, which was attributed to an increase in the surface contact area between the water droplets and the base layer. A smaller pore size with a large pore size distribution (achieved through less viscous at low speed) and a small pore size with a small pore size distribution (achieved through more viscous at low speed) enhance the contact angle. In large pore-size films, the air tension created in the air pockets is reduced, because of the escape of the air from the larger pores, resulting in a smaller water contact angle.

- (b) Homogeneity and roughness: Similarly, we observed multiple changes in homogeneity and surface roughness with alterations in the viscosity and the speed. Initially, we considered spinning a more viscous solution at a low speed that resulted in the most homogeneity or the least inhomogeneity with a very smooth surface. This smooth surface is due to the presence of higher proportions of polymer or lower proportions of solvent on the substrate and upon phase separation, the pores created are in the sub-micro range and the polymer expelled from the substrate is less resulting in a most homogenous surface with least surface roughness. When the more viscous

solution was spun at high speed, we observed the most inhomogeneous and the least homogeneity with a very rough surface. This very rough surface is due to the expulsion of more polymer from the surface, resulting in wave-like shores. The higher the mass, the more the expulsion, resulting in less polymer-occupied surfaces. This results in a very inhomogeneous and least homogeneity with very high surface roughness. Theoretically, the higher the surface roughness, the higher the contact angle, and the lower the surface roughness, the lower the contact angle. In these two cases, we observed the results in contrast, which is because the roughness of the surface is too intense that the surface contact area between the water droplets and the base layer is high resulting in a lower water contact angle. On the other hand, a low viscous solution at low speed was spun which resulted in a relatively less homogeneity and a rough surface compared to the more viscous solution spun at low speed (see Fig. 3a–d). This decrease in smoothness and increase in inhomogeneity is due to the presence of more proportions of solvents on the surface resulting in more phase-separated regions compared to the more viscous solution spun at low speed. Contrarily, the spinning of the less viscous solution at high speed resulted in a rougher surface area with a decrease in homogeneity. The homogeneity achieved in a less viscous solution at high speed is more than the homogeneity achieved in a more viscous solution at high speed. The contact angle (159°) achieved on surfaces made from less viscous solution at low speed is more than the contact angle (152°) achieved on surfaces made from less viscous solution at high speed. The contact angle (155°) achieved on surfaces made from high viscous solution at low speed is more than the contact angle (148°) achieved on surfaces made from high viscous solution at high speed. This enhanced water contact angle on superhydrophobic surfaces made from low viscous solutions at low speed is attributed to the air inside the air pockets of the pores, optimum homogeneity and surface roughness. Lastly, the spikes that are present on the surface of the superhydrophobic films resulted in the suspension of water droplets in the air and resist the fall of the droplet on the surface due to gravity, which causes water droplets to bounce back and contribute to water-repellent properties.

- (c) Similarly, the sliding angle (3.6°) achieved on surfaces made from less viscous solution at low speed is less than the sliding angle (8°) achieved on surfaces made from less viscous solution at high speed. The sliding angle (5.6°) achieved on surfaces made from high viscous solution at low speed is less than the sliding angle (10°) achieved on surfaces made from high viscous solution at high speed. This increase in the sliding

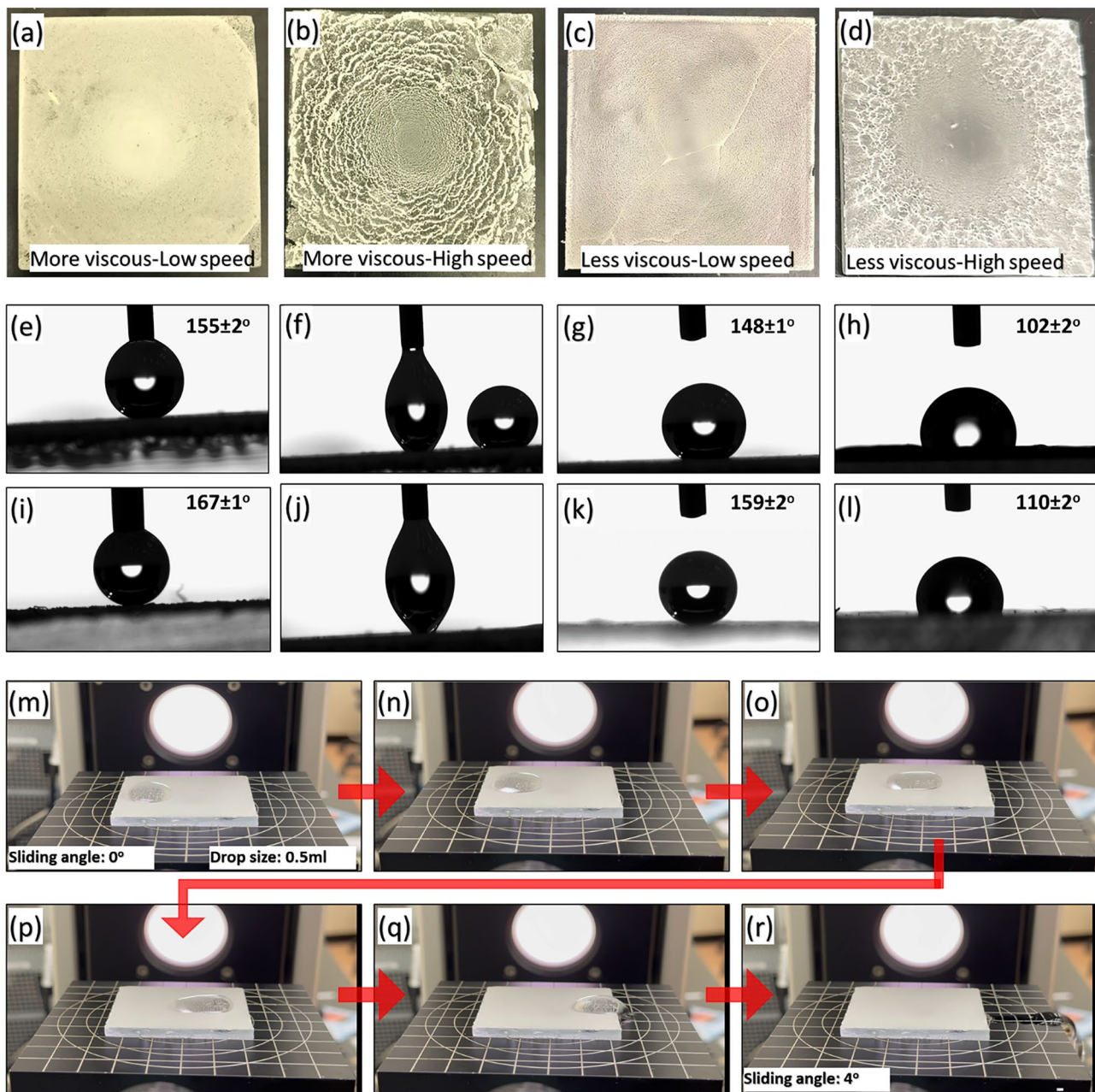


Fig. 3 **a–d** Visual manifestation of PP-Blend on different fabrication scenarios. **e–l** Contact angle with a water droplet (2 μL) on **e** HD-Blend (top surface) when the droplet is attached to the needle; **f** droplet separating from the needle on HD-Blend (top surface); **g** contact angle on HD-Blend (top surface) when the droplet is separated from the needle and freely resting on the HD-Blend top surface; **h** contact angle on the top layer of HD-Blend when heated completely; **i** PP-

Blend (top surface) when the droplet is attached to the needle; **j** droplet separating from the needle on PP-Blend (top surface); **k** contact angle on PP-Blend (top surface) when the droplet is separated from the needle and freely resting on the HD-Blend top surface; **l** contact angle on the top layer of PP-Blend when heated completely. **m–r** Visual images of sliding angle measurement of a water droplet over the PP-Blend coated glass surface

angle in the more viscous solution is due to the attraction of water droplets towards the base layer because of more pore size and pore size distribution.

- (d) An additional contributing factor to the high contact angle on surfaces made from less viscous solution at low speed is the formation of crystalloids. At high

speed, the solvent evaporates rapidly, leaving behind a pure polymer that quickly crystallizes. In contrast, at low speed, the slow evaporation of the solvent delays the process of crystallization within the polymer, resulting in the formation of uniform crystalloids that support a high contact angle.

- (e) Temperature and time of heating are crucial factors in achieving the maximum contact angle. It was observed that at room temperature (25 °C), the maximum contact angle (159°) was achieved. However, an increase in temperature resulted in a decrease in the contact angle, and this decrease was dependent on the duration of heating. Since polymers are insulators, a slight increase in temperature for a very short period does not significantly affect their state. Therefore, if the temperature is increased by 5 °C in less than five min, there will be no noticeable change in the contact angle. However, if this slight increase in temperature is maintained for a longer duration the heat is absorbed by its inner crystalline structures. These crystalloids, which contribute to the formation of spikes on the surface and support a high contact angle or water repellency, begin to diminish. Additionally, prolonged heating of the polymer leads to oxidation, also resulting in poor water repellency.

3.2 Contact angle and sliding angle measurements

Contact angle measurement is a crucial parameter that determines the extent of hydrophobicity exhibited by a surface [47]. Figure 3e–g shows the observations made on the top layer of HD-Blend while Fig. 3i–k depicts observations made on top layer of PP-Blend, see Table S1. Initially, when a water droplet was dispensed onto the HD-Blend surface using a needle from the contact angle measurement machine (see Fig. 3e), it formed a contact angle of 155° with the surface. However, it was observed that the water droplet adhered more strongly to the needle than to the surface. This resistance can be attributed to the water repellency of the surface. Subsequently, a force was applied to separate the water droplet from the needle (see Fig. 3f), resulting in a measured contact angle of 148° (see Fig. 3g), which we consider being the accurate value for the contact angle measurement in the case of HD-Blend, as it is independent of any external force. Furthermore, contact angle measurements were also conducted on the top layer of the thin film when heated completely. We will represent this heated top layer as the second layer. In this scenario, when the second layer is heated and top layer is applied, then the attachment

and interconnection between the second layer and top layer was excellent because of the same polymer. Also, the second layer acts as independent film as well as a support for the superhydrophobic thin film layer. As a result of the polymer melting process, crystalloids and spikes were diminished from this surface. Consequently, the hydrophobicity was compromised, leading to a contact angle of 102° (see Fig. 3h).

A similar procedure was followed to measure the contact angle on the PP-Blend surface. When the water droplet came into contact with the needle, a contact angle of 167° was observed (see Fig. 3i). An external force was then applied to separate the droplet from the needle (see Fig. 3j), and once the droplet became independent, PP-Blend exhibited the highest contact angle of 159° (see Fig. 3k). This superhydrophobic behavior can be attributed to the formation of spikes and crystalloids on the top surface of the PP-Blend, as discussed in the SEM section. Additionally, the hydrophobicity of the heated second layer of PP-Blend was determined. We observed a similar result as in HD-Blend, with a 110°, see Fig. 3l. We anticipated that the heated base layer will also show a very low contact angle, since the base layer of both thin films, HD-Blend and PP-Blend was the same and underwent the same heating procedure, they exhibited the same level of hydrophobicity with a contact angle of 108°.

We measured the sliding angle of the PP-Blend to determine the angle at which water droplet slides over the superhydrophobic surface. Initially, we placed a 0.5ml water droplet on the PP-Blend surface at a 0° angle (Fig. 3m). Subsequently, we gradually tilted the plate, coated with a thin film of PP-Blend, to observe the movement of the water droplet (Fig. 3n–r). We observed that the droplet began to move when the angle was increased to 2° (Fig. 3n), and it exhibited more pronounced movement at an angle of 3° (Fig. 3o). Finally, the droplet slid completely when the angle reached 4° (Fig. 3p–r). Consequently, the sliding angle of the PP-Blend thin film surface was determined to be 4°, which closely aligns with linearity and confirms its superhydrophobic nature. Additionally, it was noted that when the water droplet size was decreased to 5 µL, the sliding angle was increased to 10°. Table 2 illustrates that our superhydrophobic surface demonstrates comparable contact angle when measured

Table 2 Contact Angle (CA) comparison of various Polyfin-based superhydrophobic products

Polymer	CA	Method	Product	Ref
PP	165°	Micro–Nano-structuring	Hydrophobic Surface	[48]
Tri-layered PP–PP/PE-PP	130°	Thermal Bonding	Breathable Waterproof	[49]
Waste PP	> 150°	TIPS–Film-casting	Filtration Membrane	[50]
PP	160°	Solvent/Non-solvent	Hydrophobic Surface	[45]
PP/PVDF	155°	Vacuum Filtration	Membrane Distillation	[51]
Waste PP-HDPE-LDPE	159°	TIPS–Spin-casting	Hydrophobic Surface	Present

against the reported — state-of-the-art — superhydrophobic surfaces.

3.3 Surface roughness

The hydrophobicity of thin films can be significantly influenced by surface roughness [52]. A rough surface can induce air pockets to form between the polymer molecules and the water droplet, allowing the droplet to sit on top of the surface without wetting it. The Cassie-Baxter state, a phenomenon associated with it, causes a rise in hydrophobicity [53, 54]. On the other hand, if the surface is exceptionally smooth, water droplets can quickly saturate it and reduce the hydrophobicity of the surface.

The AFM images of the superhydrophobic thin films — HD-Blend and PP-Blend — were captured, and their root mean square (RMS) values were examined to ascertain the

surface morphology and, consequently, the degree of roughness (Fig. 4 and Table S2).

As stated in Table S2, the approximate RMS values of the top surfaces of HD-Blend and PP-Blend were 90 nm and 228 nm, respectively. Our findings demonstrated that HD-Blend, where the top layer consists of HDPE exhibited low hydrophobicity as compared to PP-Blend, where the top layer was comprised of PP.

Figure 4c–iii presents an atomic force microscopy (AFM) image of the top surface of the PP-Blend material, revealing a prominent formation of spikes. As previously discussed in the SEM section, these spikes play a crucial role in the formation of a superhydrophobic surface. In contrast, Fig. 4a–iii displays an AFM image of the top surface of the HD-Blend material, showing fewer spikes compared to the PP-Blend Thin film. Consequently, the contact angle measurement for the HD-Blend material is lower than that of the PP-Blend material.

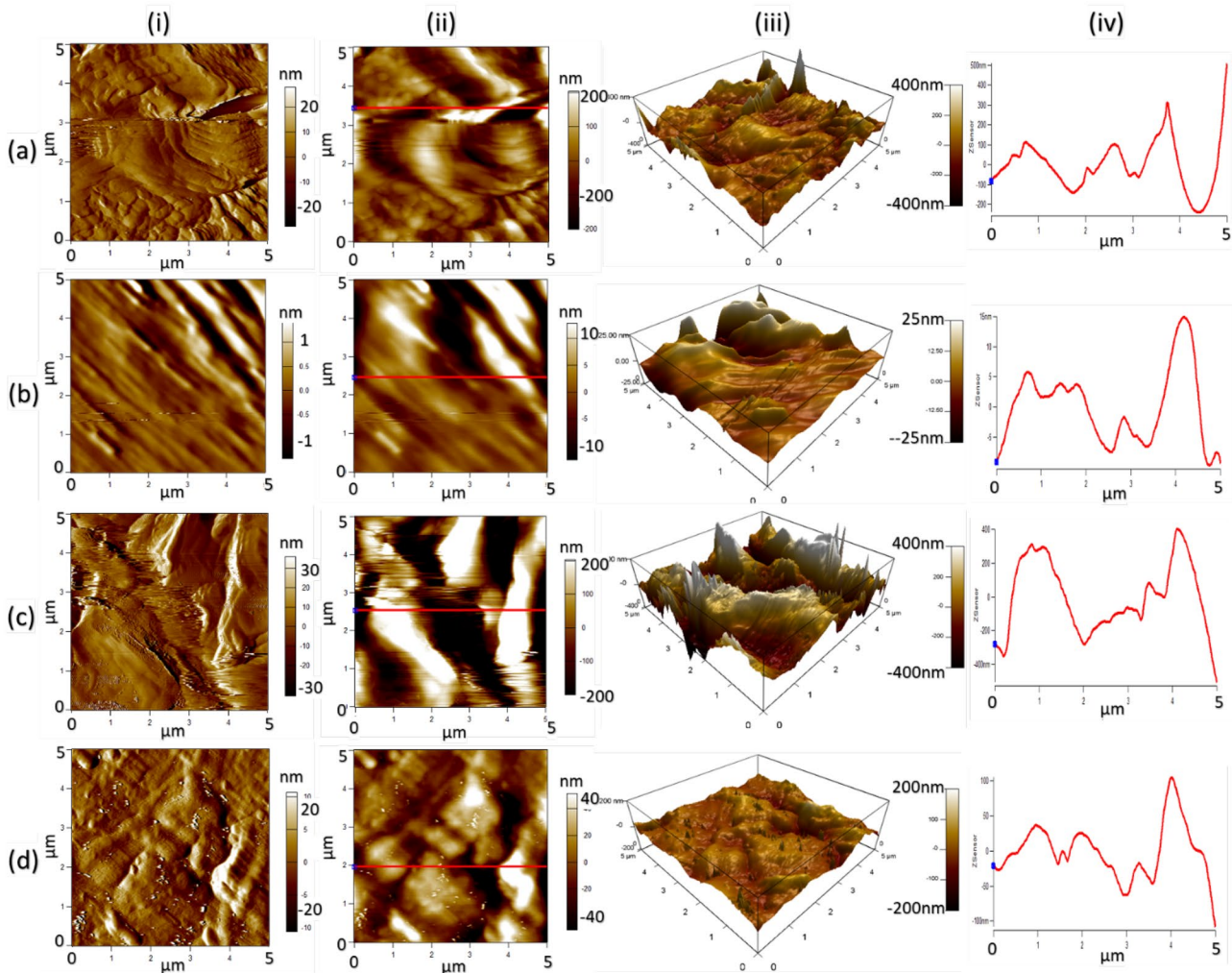


Fig. 4 AFM of **a** HD-Blend top surface **b** HD-Blend bottom surface **c** PP-Blend top surface **d** PP-Blend bottom surface; **i** amplitude retrace mode **ii** Z-sensor retrace mode **iii** 3D XYZ-axes surface roughness **iv** 2D XZ-axes profile roughness

The surface morphology of the materials played a significant role in achieving superhydrophobicity. The backside of both the PP-Blend and HD-Blend materials exhibited the least hydrophobicity, as evidenced by a contact angle of 108° , as discussed in the contact angle section. The base layers of both HD-Blend and PP-Blend were subjected to heating, resulting in the reduction of spike formation and oxidation of the polymer. As a consequence of this oxidation process, the presence of OH- groups increased within the base layer. Subsequently, this led to an increase in hydrophilicity rather than hydrophobicity, primarily due to the intermolecular forces between the OH groups and water molecules. A comprehensive analysis of this phenomenon will be provided in the XPS section. This is further supported by the AFM images of the backside surfaces (Fig. 4b–iii, d–iii), which appear smoother compared to the top surfaces. Therefore, the AFM results validate the predicted surface morphology discussed in the SEM section.

3.4 Functional group analysis of Superhydrophobic thin films

In order to estimate the inner chemistry of superhydrophobic thin films FTIR analysis was carried out and the findings are shown in Fig. 5. Since in the fabrication of superhydrophobic thin films, all the chemicals utilized are polyolefin in nature, leading to all the peaks observed in the FTIR spectra being attributed to carbon and hydrogen bonds. The Pure PP FTIR graph (Fig. 5a) displays a few distinct peaks. Specifically, three peaks were identified at 2870 cm^{-1} , 2920 cm^{-1} , and 2950 cm^{-1} , indicating the presence of CH_3 stretching, CH_2 asymmetrical stretching, and CH_3 asymmetrical stretching, respectively [55, 56]. Another distinct peak was observed at 1376 cm^{-1} , which is associated with the symmetrical bending of CH_3 of the branched methyl group.

Similarly, the characteristic peaks of HDPE and LDPE are largely identical due to their similar composition, with

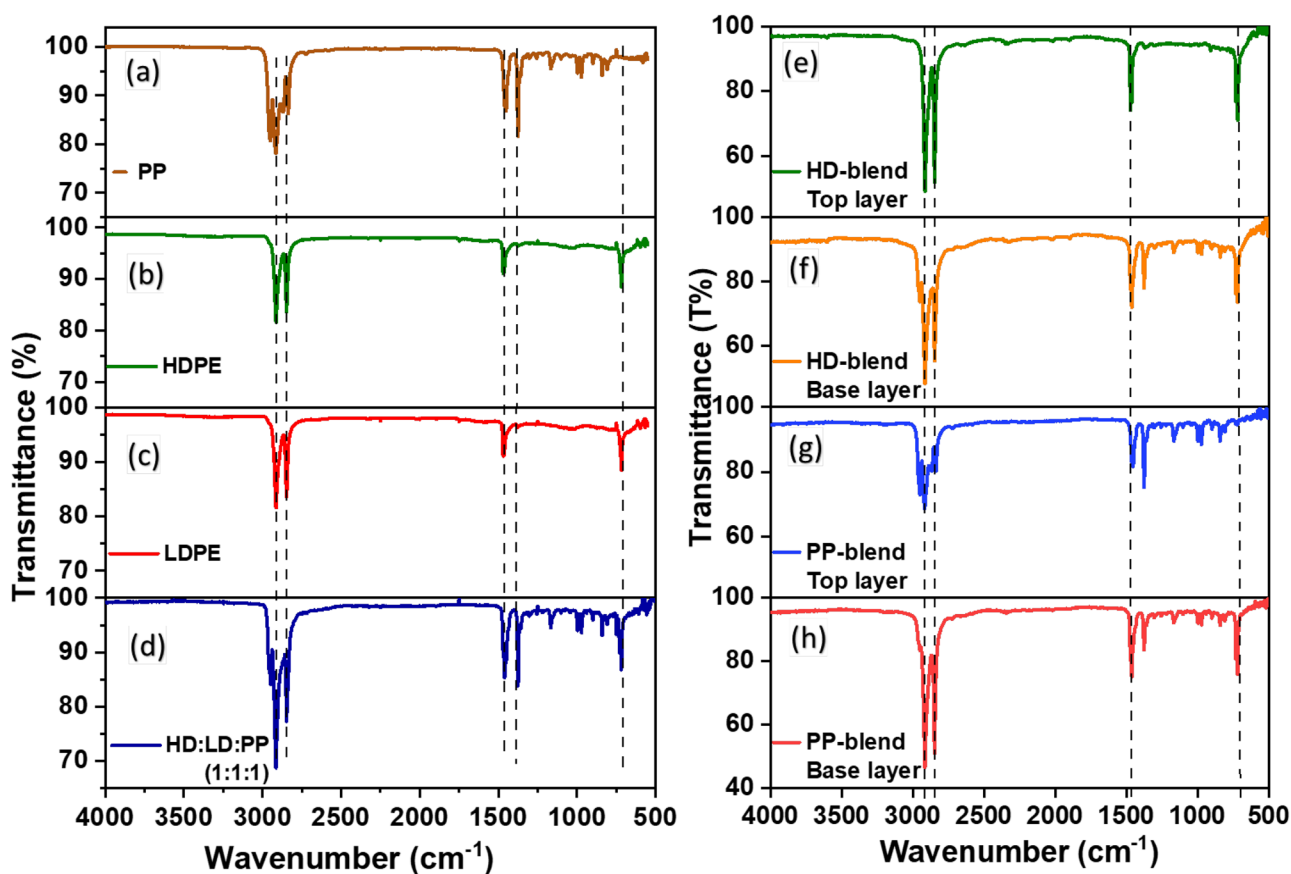


Fig. 5 FTIR of **a** pure PP **b** pure HDPE **c** pure LDPE **d** blend of polyolefins in equal ratio **e** top layer of HD-blend **f** base layer of HD-blend **g** top layer of PP blend, and **h** base layer of PP-blend

the only variation being in their densities. Peaks were detected at 2860 cm^{-1} , representing CH_2 symmetric stretching, 2920 cm^{-1} for CH_2 asymmetric stretching, 2954 cm^{-1} for asymmetric stretching, 1377 cm^{-1} for CH_3 exhibiting umbrella bending mode, and $729\text{--}720\text{ cm}^{-1}$ indicating split CH_2 rocking vibration [57] (Fig. 5b–c). Upon the formation of a polymer blend consisting of all three polyolefins in a ratio of HDPE:LDPE:PP = 1:1:1, the characteristic peaks of HDPE, LDPE, and PP were collectively observed in the polymer (Fig. 5d).

Since the base layers in HD-Blend and PP-Blend were composed of a polymer blend encompassing all three polyolefins, the characteristic peaks displayed in Fig. 5d, f, and h are relatively identical.

The confirmation of $\text{C}=\text{C}$ bonds is also evidenced by the peak at 750 cm^{-1} observed in Fig. 5e–f, specifically in the HD-Blend top and base layers. A higher proportion of $\text{C}=\text{C}$ bonds indicates a greater frequency of crosslinking within the polymer chain during the blending process. Increased crosslinking levels ultimately result in higher degrees of

crystallinity, which contribute to the strength of the polymer blend.

In the top layer of PP-Blend, three peaks were identified at 808 cm^{-1} for $\text{C}=\text{C}$ stretching, 996 cm^{-1} for CH_3 rocking, and 1166 cm^{-1} for $\text{C}=\text{C}$ wagging (Fig. 5g).

3.5 Thermal analysis of superhydrophobic thin films

To estimate the degradation temperature of developed thin films, HD-Blend and PP-Blend DSC was carried out and results are shown in Fig. 6. Figure 6a depicts the degradation curve of pure PP, which undergoes degradation at 168°C . While Fig. 6b–c illustrates the degradation curve of pure HDPE and LDPE, respectively. Pure HDPE degrades at a temperature of 124°C , whereas LDPE degrades at 110°C . It is to be noted that the higher melting temperature of PP is attributed to the branched alkyl groups. However, the semi-sharp peaks of these polymers denote their semi-crystalline nature.

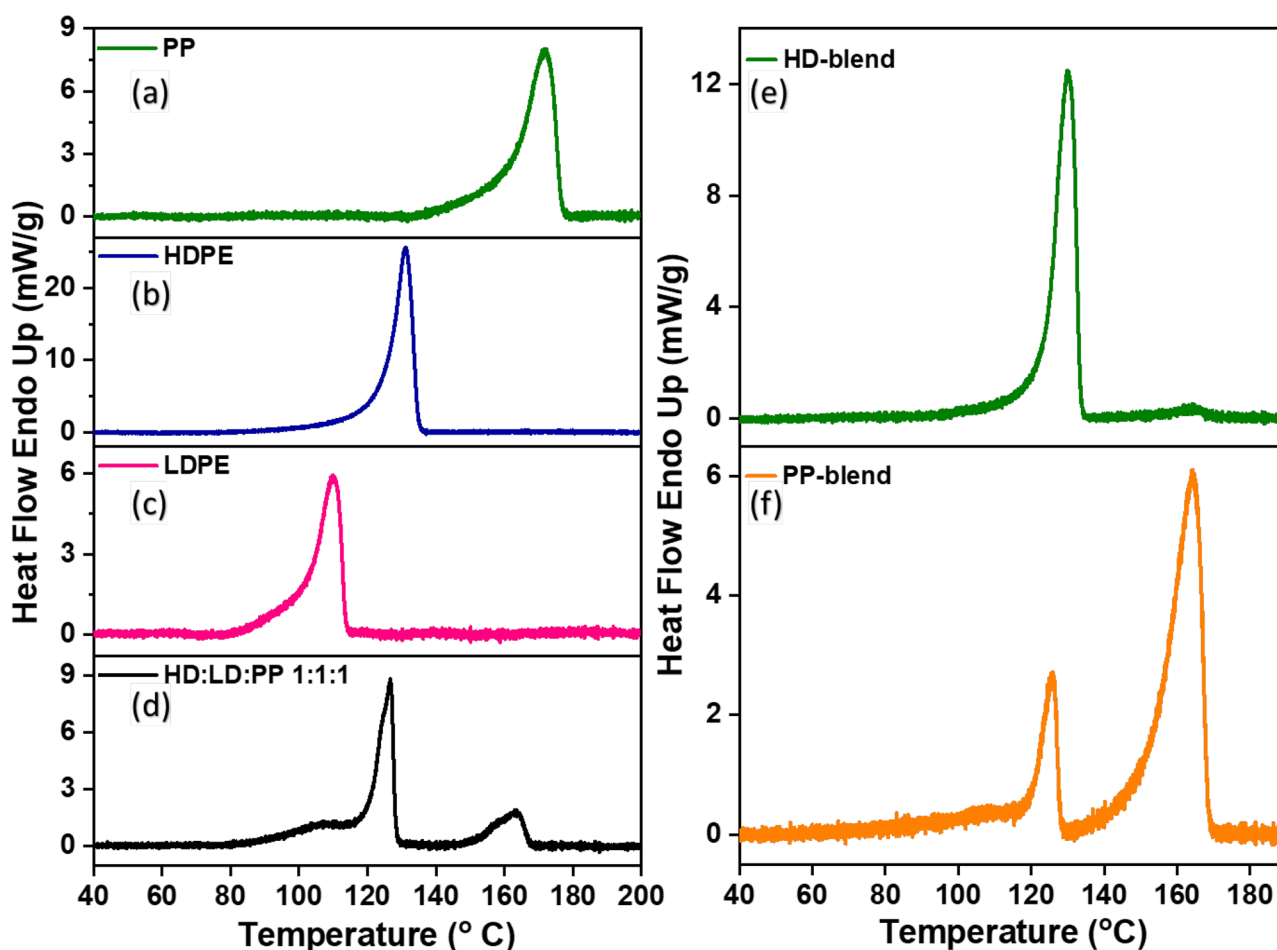


Fig. 6 Degradation curves of a pure PP b pure HDPE c pure LDPE d blend of polyolefins in equal ratio e HD-blend f PP-blend

When a blend of the aforementioned polyolefins is created, the characteristic peaks of all three compounds are observed in the DSC curve of the polymer blend (Fig. 6d). The polymer blend consists of 33% HDPE, 33% LDPE, and 33% PP. The degradation curve of HDPE and LDPE is more prominently reflected at 124 °C, whereas a smaller curve indicating the degradation of PP is observed at 164 °C. However, the LDPE peak was merged with the HDPE peak, resulting in a broader base.

Figure 6e illustrates the degradation curve of HD-Blend. Initially, significant degradation occurs at 124 °C due to the presence of 66% PE (HDPE and LDPE) in the base layer, and the top layer also consists of HDPE, the dominating polymer is polyethylene, thus, we observed a major PE peak and a very small PP peak at 164 °C.

On the other hand, PP-Blend undergoes two stages of melting. The initial one occurs at 124 °C due to the presence of HDPE and LDPE in the base layer, while the final melting occurs at 164 °C due to the high concentration of PP in the PP-Blend thin film (see Fig. 6f). This shortening of melting point is attributed to the homogenous mixing of PP with PE.

3.6 Chemical composition analysis of superhydrophobic thin films through XPS

Chemical composition analysis of fabricated thin films was carried out through XPS obtained results are shown in Fig. 7.

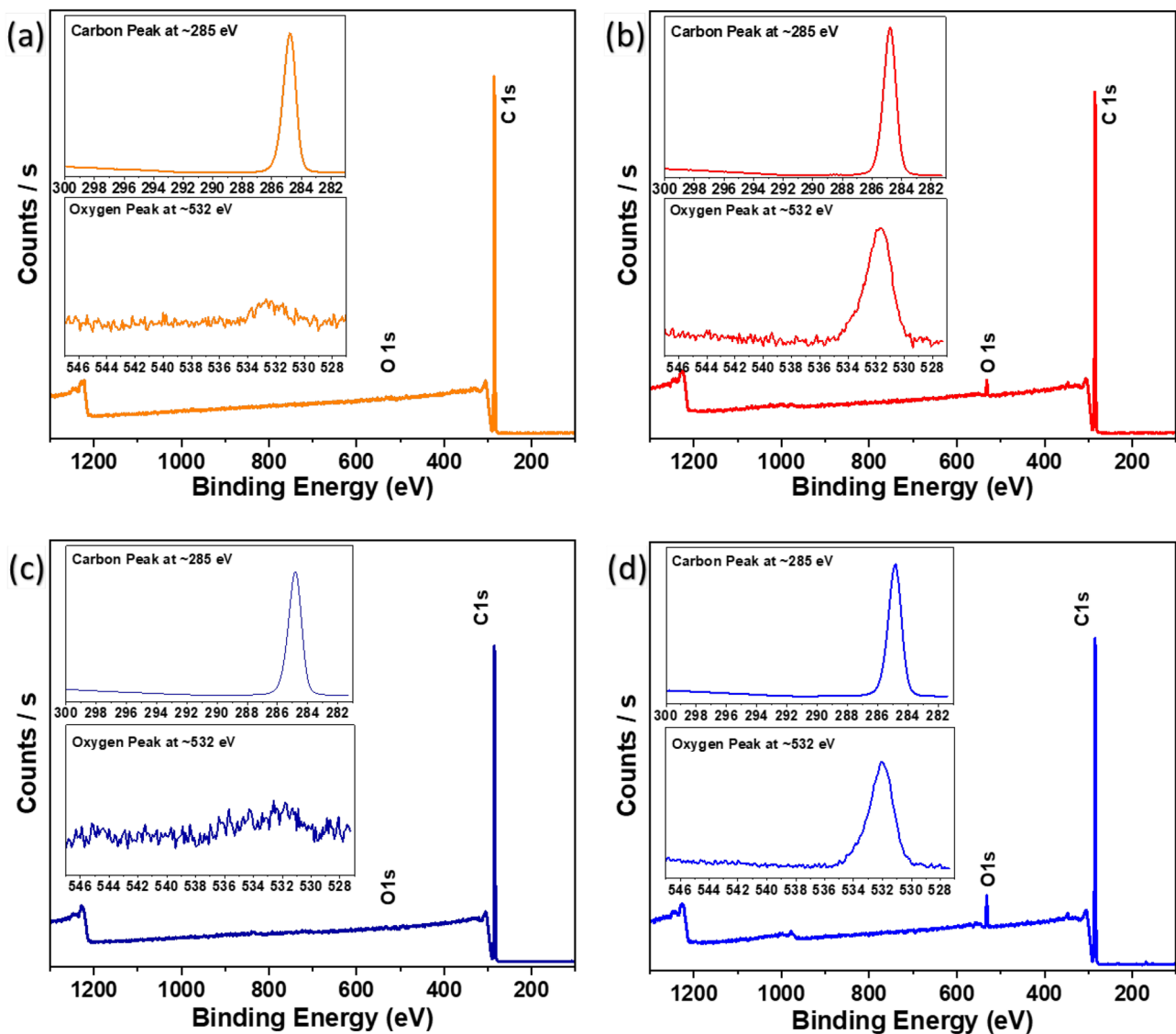


Fig. 7 XPS spectra of **a** top layer of HD-blend **b** base layer of HD-blend **c** top layer of PP-blend **d** base layer of PP-blend, (inset) Carbon 1s and Oxygen 1s spectra of respective compositions

XPS provides us the atomic composition on the surface. We initially studied the chemical composition of HD-Blend top surface and PP-blend top surface, Fig. 7a and c, respectively. As we have used xylene in our methodology, we wanted to confirm the removal of xylene from the superhydrophobic surface. Usually, the π - π^* interactions of the aromatic arene C=C is visualized at 294 eV. We did not observe any peak at 294 eV, confirming the absence of xylene in the superhydrophobic films. Moreover, the oxygen content in the top surface was negligible, and suggests the absence of hydrophilic groups such as O-H, or C-O-C groups, etc.

On the other hand, the XPS spectra of the heated thin films HD-Blend, and PP-Blend showed the presence of <2% of oxygen, which is attributed to the partial oxidation of the surface due to heating. The heating process not only reduced the surface spikes, as discussed in the SEM section, but also induced partial oxidation by the presence of C-O-C, C-C-O peaks (Fig. 7b, d). This partial oxidation resulted in the introduction of hydrophilic groups, resulting in a decrease in the contact angle with water below 110°.

The effect of annealing on the cross-linking of polymer chains is well-established in the literature [58]. Annealing increased the degree of crosslinking in the base layer by rearranging the polymer chains, resulting in enhanced mechanical strength of the base layer [58, 59]. The base layer in HD-Blend and PP-Blend are constituted of mixed plastic waste. Annealing of the base layer in HD-Blend and PP-Blend induced oxidation reactions, leading to an increase in the number of oxidized functional groups.

The presence of carbonyl groups in HD-Blend and PP-Blend is also evident in FTIR results. The presence of oxygen in HD-Blend and PP-Blend showed a significant impact on the chemical, physical properties, and surface properties [60, 61]. The base layer's oxidation produces more active sites on the surface which makes the surface more welcoming to the topcoat, leading to better adhesion. The extent of oxidation can be controlled by adjusting the annealing temperature, time, and the presence of oxidative agents.

3.7 XRD analysis of superhydrophobic thin films

X-ray diffraction analysis was conducted to investigate the crystallinity and structural properties of thin films. PP and PE exist in a semi-crystalline form. The crystallinity is observed and calculated through the area under the curve of the XRD patterns. Before that, the representative sample is identified for the presence of PP or PE or both by XRD pattern peaks. The PP and PE are identified by the presence of the characteristic peaks. PP shows peaks at 13° and 17° (2 θ), whereas the HDPE and LDPE show characteristic peaks at 22° and 24° (2 θ), see Fig. 8a–c, respectively.

The variation in intensities is attributed to the density differences between HDPE and LDPE. These relatively sharp peaks in the graphs indicate the semi-crystalline nature of HDPE and LDPE. In Fig. 8d, which represents the nature of a polymer blend utilized as a base layer in both thin films, HD-Blend and PP-Blend, two key observations are made: (a) all characteristic peaks of LDPE, HDPE, and PP are collectively present in the blend graph. (b) all peaks are relatively sharp, indicating a semi-crystallinity of the polymer blend.

When the base layer of HD-Blend was examined through XRD, characteristic peaks were obtained at 14°, 16°, 18°, 21° and 25°, see Fig. 8f. Peaks at 14°, 16°, and 18° represent the presence of PP in the base layer while peaks obtained at 21° and 25° is attributed to PE. This validates the presence of mixed plastic in the base layer of HD-Blend. Similar to this, the top layer of HD-Blend only displayed the two PE-related peaks at 21° and 25°, indicating that upper layer was constituted with HDPE (Fig. 8e). The base layer in PP-Blend is similar to HD-Blend as they both were constituted with a polymer blend of mixed polyolefins. Therefore, base layer peaks in both graphs showed similar peaks in Fig. 8f and h.

In the PP-Blend XRD pattern, top layer peaks were observed at 14°, 16°, 18°, and 22° (Fig. 8g). These peaks indicate the presence of PP [62]. The perfect mixing between the top and bottom layers in PP-Blend is confirmed by the XRD data, which is due to well-performed annealing during the fabrication process [63]. Well-blend two layers also can be seen through SEM results. This may be explained by the fact that PP-Blend performed better than HD-Blend in terms of the hydrophobicity properties [64].

3.8 Mechanical properties of hydrophobic multilayered thin films

Like any other polymer, the structural morphology and packing of multilayer hydrophobic thin films strongly influenced their mechanical properties. The results of mechanical testing (Young modulus and Tensile strengths (Fig. 9), of thin films, showed the expected behavior as per their morphology, as discussed in the SEM results section.

In this work, the strength for the superhydrophobic films is achieved by the heating of the base layer, which has LDPE, HDPE, and PP. The elasticity of LDPE is more than HDPE, which is more than PP. The base layer plays a major role in achieving the tensile strength, as the base layer is significantly heated and the polymer chains are compactly arranged. In contrast, the top superhydrophobic layer plays a mild role in tensile strength as it is porous and the loose packing of the polymer chains, but it binds to the base layer to avoid the chipping property. It was observed that the strength of PP-blend is relatively strong than the HD-blend, because of the more strength and rigid nature

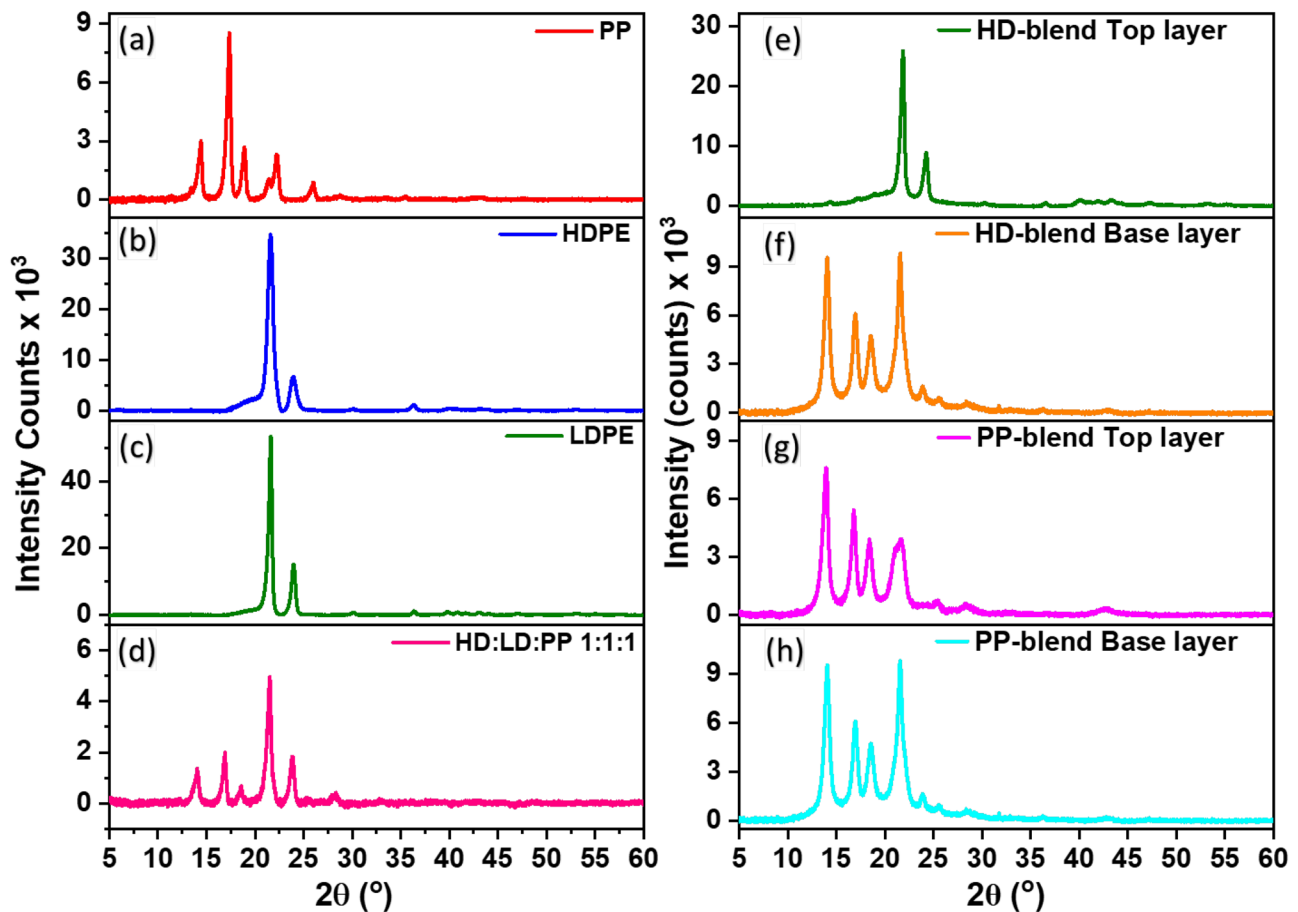
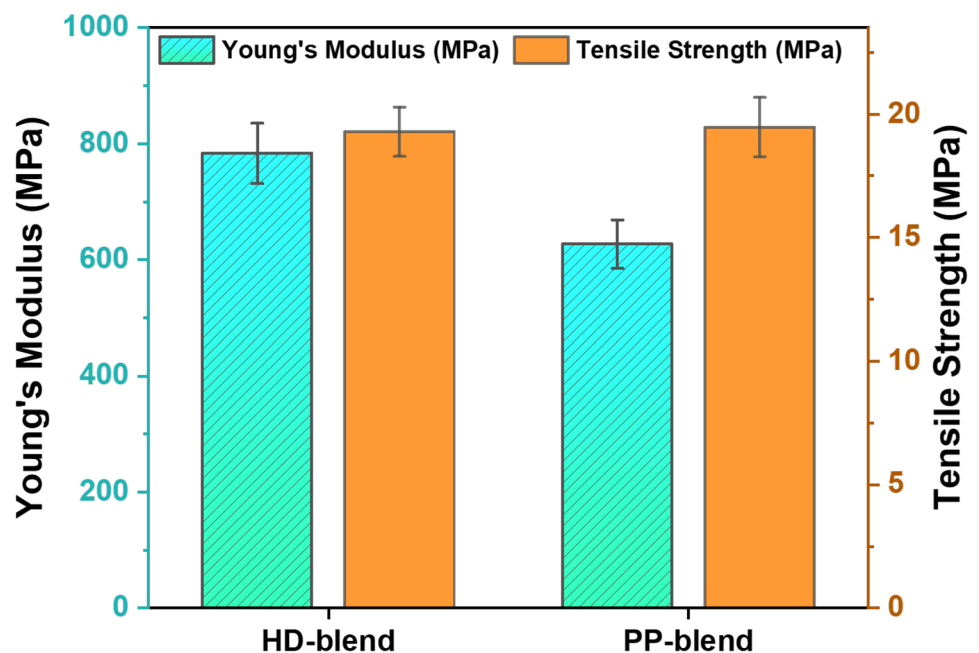


Fig. 8 XRD patterns of **a** pure PP **b** pure HDPE **c** pure LDPE **d** blend of polyolefins in equal ratio **e** top layer of HD-blend **f** base layer of HD-blend **g** top layer of PP blend **h** base layer of PP-blend

of the PP, whereas the HDPE has relatively lesser strength and is more flexible. The modulus of the PP-blend is less because of more rigidness of PP, and it breaks relatively

suddenly instead of elongating for some distance. In contrast, the HDPE has more elasticity and has more degree of elongation, thus, the modulus is more for the HD-Blend.

Fig. 9 Mechanical properties of HD-blend and PP-blend hydrophobic films



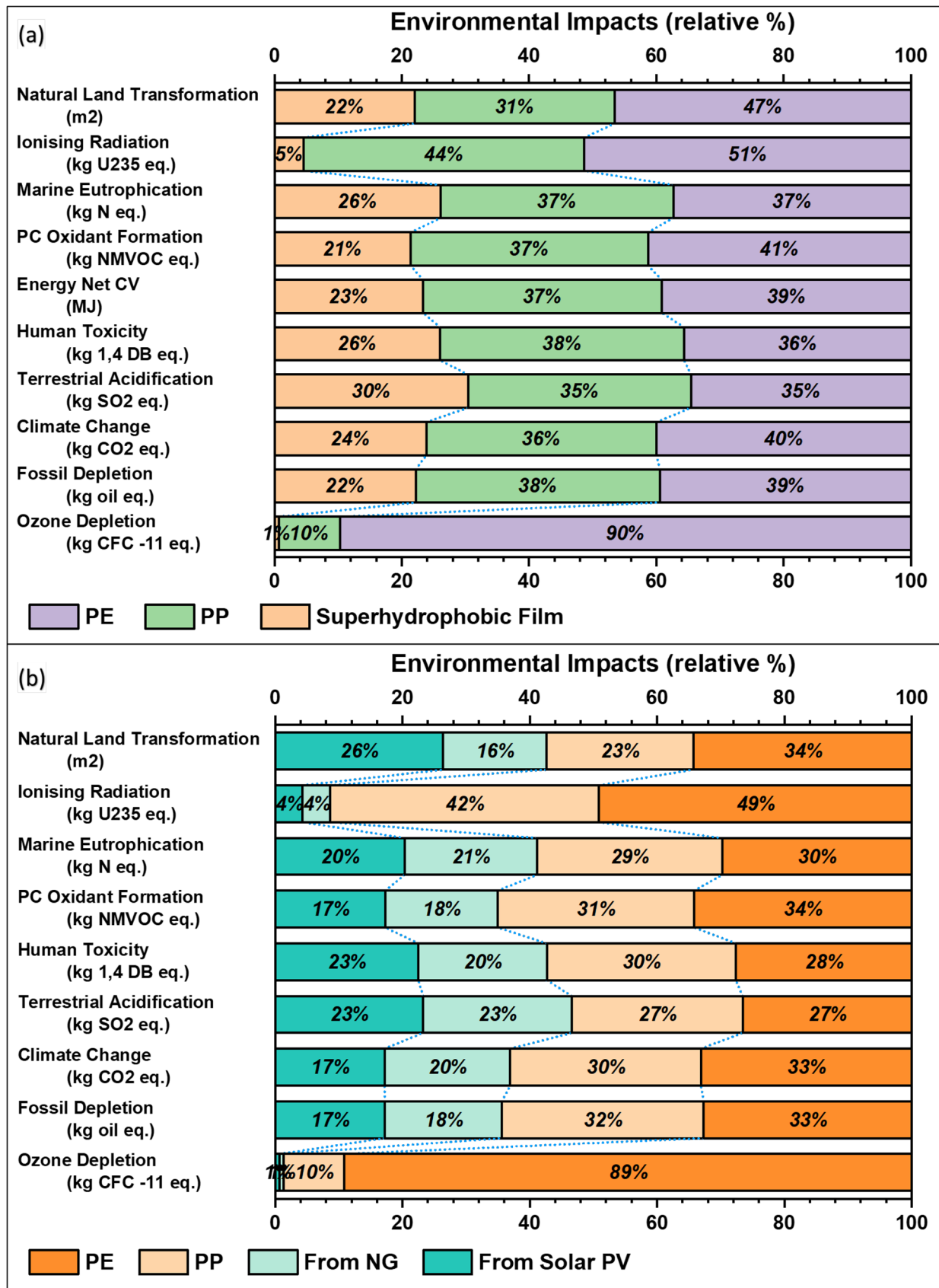


Fig. 10 **a** Comparison of normalized environmental impacts of superhydrophobic film produced from plastic waste with virgin pellets of PP and PE from petroleum source; and **b** comparison of normalized environmental impacts using natural gas and solar PV as electricity sources

The average tensile strength of HD-Blend and PP-Blend was recorded at 19.27 MPa and 19.47 MPa respectively.

3.9 LDPE based hydrophobic multilayered thin films

During the segregation process of mixed plastic waste through the float sink method, three types of polyolefins were obtained (i) polypropylene (PP), (ii) High density polyethylene (HDPE), and, (iii) Low density polyethylene (LDPE). Initially we designed hydrophobic multilayered thin films using all aforementioned three types of polyolefins as the top layer. However, the hydrophobicity test and contact angle measurements for the thin film that was created using LDPE as the top layer and a polymer blend as the base layer did not show any appreciable findings. The contact angle in LDPE thin films was obtained at 122° which was not up to par, so further characterization was omitted for this thin film.

As Low-density polyethylene (LDPE) has ethylene polymeric chains with a high degree of branching, leading to a highly amorphous structure with a low degree of crystallinity [65]. The molecular packing in LDPE is characterized by randomly coiled chains that have a high degree of entanglement. As a result, the intermolecular forces in LDPE are weak, and the polymer has low strength and stiffness compared to other polyethylene types. The amorphous regions within the LDPE structure offer little resistance to the movement of molecules, allowing them to pass through with ease. In contrast, high-density polyethylene (HDPE) has a high degree of crystallinity and a more tightly packed molecular structure due to the use of linear ethylene chains without branching. The intermolecular forces in HDPE and PP are stronger than in LDPE, leading to higher strength, stiffness, and resistance to deformation [66–68]. Additionally, the higher degree of crystallinity in HDPE and PP reduces its permeability to gases, liquids, and vapors, making it a more suitable material for multilayer thin film hydrophobic films.

3.10 Life cycle assessment

A Life Cycle Assessment (LCA) was conducted to evaluate the environmental impacts of producing 1 kg of superhydrophobic films using our synthesis method. The production route is depicted in Fig. S2. Various environmental factors were considered, including embodied energy, ozone depletion, fossil fuel depletion, marine eutrophication, climate change (total carbon emissions), total embedded energy,

ionizing radiation, and natural land transformation. To estimate these LCA indicators, we utilized the commercial software tool Gabi. Environmental impacts of superhydrophobic film produced from plastic waste was compared with virgin pellets of PP and PE produced from petroleum source, based on equal weight. Additionally, we examined the environmental effects of utilizing electricity from solar PV in comparison to natural gas.

The findings revealed a 12% and 16% reduction in carbon footprint compared to the production of virgin PP and PE, respectively. Moreover, a decrease of 16% in embodied energy was observed when compared to the synthesis route of virgin PP and a 17% decrease was recorded when compared to the synthesis route of virgin PE. Overall, the results suggest that open-loop recycling is more favorable in terms of lower carbon footprints and embodied energy when compared to the traditional petroleum-derived synthesis route (Fig. 10a).

3.10.1 Effects of renewable energy

The utilization of solar photovoltaic (PV) electricity was compared with the use of natural gas, with the objective of enhancing the eco-friendliness of the recycling process (Fig. 10b). The incorporation of solar PV sources leads to an additional reduction in various environmental indicators. A depletion rate of 17% was observed for solar PV, 23% for natural gas, 32% for virgin PP synthesis, and 33% for virgin PE synthesis in terms of fossil resources. Likewise, the total carbon footprint associated with solar PV was found to be 17%, while natural gas accounted for 20% of the total carbon footprint. The synthesis of virgin PP resulted in a carbon footprint of 30%, whereas PE synthesis yielded a carbon footprint of 33%. Therefore, the implementation of solar PV shows positive results in reducing gross environmental impacts.

4 Conclusion

We present a strategy in which mixed plastic waste is converted into free-standing superhydrophobic films through selective dissolution, thermally induced phase separation, controlled spin-casting, and annealing. This approach is demonstrated using mixtures of HDPE, LDPE, and PP, which are among the most abundant components of post-consumer plastic waste. We synthesized a two-layered superhydrophobic thin film with high surface roughness and sufficient mechanical strength, making it suitable for use as a free-standing material. The contact and sliding angles were found to be 159° and 4° , respectively, with an RMS surface roughness of 228 nm. Additionally, the life cycle assessment revealed that the production of superhydrophobic films

via the open-loop recycling method is better than virgin PP and PE produced from petroleum in terms of carbon dioxide emissions and embodied energy. Our design approach not only results in the creation of a superhydrophobic product but also offers an alternative method for recycling plastic waste without the need for expensive sorting techniques.

Supplementary Information The online version contains supplementary material available at <https://doi.org/10.1007/s42114-024-00829-2>.

Author contributions Junaid Saleem and Zubair Khalid wrote the main manuscript text. Junaid Saleem and Zubair Khalid prepared all the figures. Junaid Saleem, Zubair Khalid, Sun Luyi, and Gordon McKay edited and reviewed the main manuscript text.

Funding Open Access funding provided by the Qatar National Library. This publication was made possible by NPRP grant number NPRP12S-0325-190443 from the Qatar National Research Fund (a member of the Qatar Foundation). Open access funding is provided by Qatar National Library.

Data availability The authors declare that the data supporting the findings of this study are available within the paper and its Supplementary Information files. Should any raw data files be needed in another format they are available from the corresponding author upon reasonable request.

Declarations

Competing interests The authors declare no competing interests.

Open Access This article is licensed under a Creative Commons Attribution 4.0 International License, which permits use, sharing, adaptation, distribution and reproduction in any medium or format, as long as you give appropriate credit to the original author(s) and the source, provide a link to the Creative Commons licence, and indicate if changes were made. The images or other third party material in this article are included in the article's Creative Commons licence, unless indicated otherwise in a credit line to the material. If material is not included in the article's Creative Commons licence and your intended use is not permitted by statutory regulation or exceeds the permitted use, you will need to obtain permission directly from the copyright holder. To view a copy of this licence, visit <http://creativecommons.org/licenses/by/4.0/>.

References

- Lebreton L, Andrady A (2019) Future scenarios of global plastic waste generation and disposal. *Palgrave Commun* 5:1–11. <https://doi.org/10.1057/s41599-018-0212-7>
- Mishra S, Charan Rath C, Das AP (2019) Marine microfiber pollution: A review on present status and future challenges. *Mar Pollut Bull* 140:188–197. <https://doi.org/10.1016/j.marpolbul.2019.01.039>
- MacArthur DE (2014) Rethinking the future of plastics the new plastics economy. *Ellen MacArthur Found.* 1–120
- Gruter GJM (2023) Using carbon above the ground as feedstock to produce our future polymers. *Curr Opin Green Sustain Chem* 40:100743. <https://doi.org/10.1016/j.cogsc.2022.100743>
- Sezgin H, Yalcin-Enis I (2021) Turning plastic wastes into textile products. *Handb Solid Waste Manag.* https://doi.org/10.1007/978-981-15-7525-9_105-1
- Jehanno C, Alty JW, Roosen M, De Meester S, Dove AP, Chen EY-X, Leibfarth FA, Sardon H (2022) Critical advances and future opportunities in upcycling commodity polymers. *Nature* 603:803–814. <https://doi.org/10.1038/s41586-021-04350-0>
- Pan D, Su F, Liu H, Liu C, Umar A, Castañeda L, Algadi H, Wang C, Guo Z (2021) Research progress on catalytic pyrolysis and reuse of waste plastics and petroleum sludge. *ES Mater Manuf.* <https://doi.org/10.30919/esmm5f415>
- Singh MV (2021) Conversions of waste tube-tyres (WTT) and waste polypropylene (WPP) into diesel fuel through catalytic pyrolysis using base SrCO₃. *Eng Sci.* <https://doi.org/10.30919/es8d1158>
- Maddodi BS, Lathashri UA, Devesh S, Rao AU, Shenoy GB, Wijerathne HT, Sooriyaperkasam N, Prasanna Kumar M (2022) Repurposing plastic wastes in non-conventional engineered wood building bricks for constructional application – a mechanical characterization using experimental and statistical analysis. *Eng Sci.* <https://doi.org/10.30919/es8d696>
- Al-Salem SM, Lettieri P, Baeyens J (2009) Recycling and recovery routes of plastic solid waste (PSW): a review. *Waste Manag* 29:2625–2643. <https://doi.org/10.1016/j.wasman.2009.06.004>
- Aznar MP, Caballero MA, Sancho JA, Francés E (2006) Plastic waste elimination by co-gasification with coal and biomass in fluidized bed with air in pilot plant. *Fuel Process Technol* 87:409–420. <https://doi.org/10.1016/j.fuproc.2005.09.006>
- Ragaert K, Delva L, Van Geem K (2017) Mechanical and chemical recycling of solid plastic waste. *Waste Manag* 69:24–58. <https://doi.org/10.1016/j.wasman.2017.07.044>
- Sullivan KP, Werner AZ, Ramirez KJ, Ellis LD, Bussard JR, Black BA, Brandner DG, Bratti F, Buss BL, Dong X, Haugen SJ, Ingraham MA, Konev MO, Michener WE, Miscall J, Pardo I, Woodworth SP, Guss AM, Román-Leshkov Y, Stahl SS, Beckham GT (2022) Mixed plastics waste valorization through tandem chemical oxidation and biological funneling. *Science* 378:207–211. <https://doi.org/10.1126/science.abo4626>
- Rahimi AR, García JM (2017) Chemical recycling of waste plastics for new materials production. *Nat Rev Chem* 1:1–11. <https://doi.org/10.1038/s41570-017-0046>
- Geyer B, Röhner S, Lorenz G, Kandelbauer A (2014) Designing oligomeric ethylene terephthalate building blocks by chemical recycling of polyethylene terephthalate. *J Appl Polym Sci.* <https://doi.org/10.1002/app.39786>
- Fukushima K, Liu S, Wu H, Engler AC, Coady DJ, Maune H, Pitera J, Nelson A, Wiradharma N, Venkataraman S, Huang Y, Fan W, Ying JY, Yang YY, Hedrick JL (2013) Supramolecular high-aspect ratio assemblies with strong antifungal activity. *Nat Commun* 4:2861. <https://doi.org/10.1038/ncomms3861>
- Zhang J, Yan B, Wan S, Kong Q (2013) Converting polyethylene waste into large scale one-dimensional Fe₃O₄@C composites by a facile one-pot process. *Ind Eng Chem Res* 52:5708–5712. <https://doi.org/10.1021/ie4004392>
- Kathalewar M, Dhapatkar N, Pacharane B, Sabnis A, Raut P, Bhawe V (2013) Chemical recycling of PET using neopentyl glycol: Reaction kinetics and preparation of polyurethane coatings. *Prog Org Coatings* 76:147–156. <https://doi.org/10.1016/j.porgcoat.2012.08.023>
- Kim HT, Kim JK, Cha HG, Kang MJ, Lee HS, Khang TU, Yun EJ, Lee D-H, Song BK, Park SJ (2019) Biological valorization of poly (ethylene terephthalate) monomers for upcycling waste PET. *ACS Sustain Chem Eng* 7:19396–19406
- Gong J, Liu J, Jiang Z, Chen X, Wen X, Mijowska E, Tang T (2014) Converting mixed plastics into mesoporous hollow carbon spheres with controllable diameter. *Appl Catal B Environ* 152–153:289–299. <https://doi.org/10.1016/j.apcatb.2014.01.051>
- Gong J, Liu J, Wen X, Jiang Z, Chen X, Mijowska E, Tang T (2014) Upcycling waste polypropylene into graphene flakes

- on organically modified montmorillonite. *Ind Eng Chem Res* 53:4173–4181. <https://doi.org/10.1021/ie4043246>
22. Zhang F, Zeng M, Yappert RD, Sun J, Lee Y-H, LaPointe AM, Peters B, Abu-Omar MM, Scott SL (2020) Polyethylene upcycling to long-chain alkylaromatics by tandem hydrogenolysis/aromatization. *Science* 370:437–441. <https://doi.org/10.1126/science.abc5441>
 23. Sullivan KP, Werner AZ, Ramirez KJ, Ellis LD, Bussard JR, Black BA, Brandner DG, Bratti F, Buss BL, Dong X (2022) Mixed plastics waste valorization through tandem chemical oxidation and biological funneling. *Science* 378:207–211
 24. Ellis LD, Orski SV, Kenlaw GA, Norman AG, Beers KL, Román-Leshkov Y, Beckham GT (2021) Tandem heterogeneous catalysis for polyethylene depolymerization via an olefin-intermediate process. *ACS Sustain Chem Eng* 9:623–628. <https://doi.org/10.1021/acssuschemeng.0c07612>
 25. Tournier V, Topham CM, Gilles A, David B, Folgoas C, Moya-Leclair E, Kamionka E, Desrousseaux M-L, Texier H, Gavalda S (2020) An engineered PET depolymerase to break down and recycle plastic bottles. *Nature* 580:216–219
 26. Ügdüler S, Van Geem KM, Roosen M, Delbeke EIP, De Meester S (2020) Challenges and opportunities of solvent-based additive extraction methods for plastic recycling. *Waste Manag* 104:148–182. <https://doi.org/10.1016/j.wasman.2020.01.003>
 27. Saleem J, Tahir F, Baig MZK, Al-Ansari T, McKay G (2023) Assessing the environmental footprint of recycled plastic pellets: a life-cycle assessment perspective. *Environ Technol Innov* 32:103289. <https://doi.org/10.1016/j.eti.2023.103289>
 28. Lang XH, Zhu TY, Zou L, Prakashan K, Zhang ZX (2019) Fabrication and characterization of polypropylene aerogel material and aerogel coated hybrid materials for oil-water separation applications. *Prog Org Coatings* 137:105370. <https://doi.org/10.1016/j.porgcoat.2019.105370>
 29. Nguyen NB, Ly NH, Tran HN, Son SJ, Joo S, Vasseghian Y, Osman SM, Luque R (2023) Transparent oil-water separating spiky SiO₂ nanoparticle supramolecular polymer superhydrophobic coatings. *Small Methods* 7:2201257
 30. Ye H, Zhu L, Li W, Liu H, Chen H (2017) Simple spray deposition of a water-based superhydrophobic coating with high stability for flexible applications. *J Mater Chem A* 5:9882–9890
 31. Saleem J, Safdar Hossain S, Moghal ZKB, McKay G (2023) Method to prepare superhydrophobic sheets from virgin and waste polypropylene. US Patent 11840609. <https://www.freepatentsonline.com/11840609.html>. Accessed 12 Dec 2023
 32. Luo J, Huo L, Wang L, Huang X, Li J, Guo Z, Gao Q, Hu M, Xue H, Gao J (2020) Superhydrophobic and multi-responsive fabric composite with excellent electro-photo-thermal effect and electromagnetic interference shielding performance. *Chem Eng J* 391:123537. <https://doi.org/10.1016/j.cej.2019.123537>
 33. Hao Y, Leng Z, Yu C, Xie P, Meng S, Zhou L, Li Y, Liang G, Li X, Liu C (2023) Ultra-lightweight hollow bowl-like carbon as microwave absorber owning broad band and low filler loading. *Carbon N Y* 212:118156. <https://doi.org/10.1016/j.carbon.2023.118156>
 34. Fan G, Wang Z, Sun K, Liu Y, Fan R (2021) Doped ceramics of indium oxides for negative permittivity materials in MHz-kHz frequency regions. *J Mater Sci Technol* 61:125–131. <https://doi.org/10.1016/j.jmst.2020.06.013>
 35. Fan G, Wang Z, Ren H, Liu Y, Fan R (2021) Dielectric dispersion of copper/rutile cermets: dielectric resonance, relaxation, and plasma oscillation. *Scr Mater* 190:1–6. <https://doi.org/10.1016/j.scriptamat.2020.08.027>
 36. Zhou S, Ding X, Wu L (2013) Fabrication of ambient-curable superhydrophobic fluoropolysiloxane/TiO₂ nanocomposite coatings with good mechanical properties and durability. *Prog Org Coatings* 76:563–570
 37. Wu B, Cui X, Jiang H, Wu N, Peng C, Hu Z, Liang X, Yan Y, Huang J, Li D (2021) A superhydrophobic coating harvesting mechanical robustness, passive anti-icing and active de-icing performances. *J Colloid Interface Sci* 590:301–310
 38. Qin LM, Chu Y, Zhou X, Pan QM (2019) Fast healable superhydrophobic material. *ACS Appl Mater Interfaces* 11:29388–29395
 39. Zhang L, Zhou AG, Sun BR, Chen KS, Yu H-Z (2021) Functional and versatile superhydrophobic coatings via stoichiometric silanization. *Nat Commun* 12:982
 40. Xu L, Jin H, Wu D, Liu B, Zhang M (2021) Superhydrophobic polystyrene coating based on phase separation of raspberry structure particle. *Colloid Polym Sci* 299:1695–1702
 41. Wang Z, Gao X, Wen G, Tian P, Zhong L, Gou X, Guo Z (2018) Robust silicon dioxide@ epoxy resin micronanosheet superhydrophobic omniphobic protective coating for applications. *Colloids Surfaces A Physicochem Eng Asp* 550:9–19
 42. Zhang G, Xie Q, Chi J, Chen Y, Zheng H, Ma C, Zhang G (2021) Tree root-inspired robust superhydrophobic coatings with high permeation for porous structures. *Iscience* 24:103197
 43. Lee D-E, Choi E-Y, Yang H-J, Murthy ASN, Singh T, Lim J-M, Im J (2019) Highly stretchable superhydrophobic surface by silica nanoparticle embedded electrospun fibrous mat. *J Colloid Interface Sci* 555:532–540
 44. Wu Y, Zhao M, Guo Z (2017) Robust, heat-resistant and multifunctional superhydrophobic coating of carbon microflowers with molybdenum trioxide nanoparticles. *J Colloid Interface Sci* 506:649–658
 45. Erbil HY, Demirel AL, Avci Y, Mert O (2003) Transformation of a simple plastic into a superhydrophobic surface. *Science* 299:1377–1380. <https://doi.org/10.1126/science.1078365>
 46. Utracki LA (2000) *Polymer Blends Handbook*, Springer. <https://link.springer.com/referencework/10.1007/0-306-48244-4>
 47. Van der Mei HC, Bos R, Busscher HJ (1998) A reference guide to microbial cell surface hydrophobicity based on contact angles. *Colloids Surfaces B Biointerfaces* 11:213–221
 48. Puukilainen E, Rasilainen T, Suvanto M, Pakkanen TA (2007) Superhydrophobic polyolefin surfaces: controlled micro- and nanostructures. *Langmuir* 23:7263–7268. <https://doi.org/10.1021/la063588h>
 49. Zhang H, Zhai Q, Cao Y, Hu J, Zhen Q, Qian X (2023) Design and facile manufacturing of tri-layer laminated polyolefin micro-fibrous fabrics with tailoring pore size for enhancing waterproof breathable performance. *Mater Des* 228:111829. <https://doi.org/10.1016/j.matdes.2023.111829>
 50. Ramírez-Martínez M, Aristizábal SL, Szekely G, Nunes SP (2023) Bio-based solvents for polyolefin dissolution and membrane fabrication: from plastic waste to value-added materials. *Green Chem* 25:966–977. <https://doi.org/10.1039/D2GC03181G>
 51. Deng L, Li P, Liu K, Wang X, Hsiao BS (2019) Robust superhydrophobic dual layer nanofibrous composite membranes with a hierarchically structured amorphous polypropylene skin for membrane distillation. *J Mater Chem A* 7:11282–11297. <https://doi.org/10.1039/C9TA02662B>
 52. Yang C, Tartaglino U, Persson BNJ (2006) Influence of surface roughness on superhydrophobicity. *Phys Rev Lett* 97:116103
 53. Miwa M, Nakajima A, Fujishima A, Hashimoto K, Watanabe T (2000) Effects of the surface roughness on sliding angles of water droplets on superhydrophobic surfaces. *Langmuir* 16:5754–5760
 54. McHale G, Newton MI, Shirtcliffe NJ (2005) Water-repellent soil and its relationship to granularity, surface roughness and hydrophobicity: a materials science view. *Eur J Soil Sci* 56:445–452
 55. Fang J, Zhang L, Sutton D, Wang X, Lin T (2012) Needleless Melt-Electrospinning of Polypropylene Nanofibres. *J Nanomater* 2012:1–9. <https://doi.org/10.1155/2012/382639>

56. Saleem J, Moghal ZKB, McKay G (2023) Up-cycling plastic waste into swellable super-sorbents. *J Hazard Mater* 453:131356. <https://doi.org/10.1016/j.jhazmat.2023.131356>
57. Saleem J, Moghal ZKB, Luyt AS, Shakoor RA, McKay G (2023) Free-standing porous and nonporous polyethylene thin films using spin coating: an alternate to the extrusion-stretching process. *ACS Appl Polym Mater* 5:2177–2184. <https://doi.org/10.1021/acsapm.2c02183>
58. Lei Y-G, Cheung Z-L, Ng K-M, Li L, Weng L-T, Chan C-M (2003) Surface chemical and morphological properties of a blend containing semi-crystalline and amorphous polymers studied with ToF-SIMS, XPS and AFM. *Polymer (Guildf)* 44:3883–3890. [https://doi.org/10.1016/S0032-3861\(03\)00328-8](https://doi.org/10.1016/S0032-3861(03)00328-8)
59. Wei QF, Mather RR, Fotheringham AF (2005) Oil removal from used sorbents using a biosurfactant. *Bioresour Technol* 96:331–334. <https://doi.org/10.1016/j.biortech.2004.04.005>
60. Takayama T, Todo M, Tsuji H (2011) Effect of annealing on the mechanical properties of PLA/PCL and PLA/PCL/LTI polymer blends. *J Mech Behav Biomed Mater* 4:255–260
61. Kietzke T, Shin RYC, Egbe DAM, Chen Z-K, Sellinger A (2007) Effect of annealing on the characteristics of organic solar cells: polymer blends with a 2-vinyl-4, 5-dicyanoimidazole derivative. *Macromolecules* 40:4424–4428
62. Alateyah AI (2018) Thermal properties and morphology of polypropylene based on exfoliated graphite nanoplatelets/nanomagnesium oxide. *Open Eng* 8:432–439
63. Bell JR, Chang K, López-Barrón CR, Macosko CW, Morse DC (2010) Annealing of cocontinuous polymer blends: effect of block copolymer molecular weight and architecture. *Macromolecules* 43:5024–5032
64. Anto T, Rejeesh CR (2023) Synthesis and characterization of recycled HDPE polymer composite reinforced with nano-alumina particles. *Mater Today Proc* 72:3177–3182. <https://doi.org/10.1016/j.matpr.2022.11.190>
65. Zhao M, Ding X, Mi J, Zhou H, Wang X (2017) Role of high-density polyethylene in the crystallization behaviors, rheological property, and supercritical CO₂ foaming of poly (lactic acid). *Polym Degrad Stab* 146:277–286
66. Pinheiro LA, Chinelatto MA, Canevarolo SV (2004) The role of chain scission and chain branching in high density polyethylene during thermo-mechanical degradation. *Polym Degrad Stab* 86:445–453
67. Lu X, Zhang J, Zhang C, Han Y (2005) Low-density polyethylene (LDPE) surface with a wettability gradient by tuning its microstructures. *Macromol Rapid Commun* 26:637–642
68. Tompkins BD, Fisher ER (2015) Evaluation of polymer hydrophobic recovery behavior following H₂O plasma processing. *J Appl Polym Sci* 132

Publisher's Note Springer Nature remains neutral with regard to jurisdictional claims in published maps and institutional affiliations.